



The protective role of autophagy in nephrotoxicity induced by bismuth nanoparticles through AMPK/mTOR pathway

Yongming Liu, Huan Yu, Xihui Zhang, Yong Wang, Zhentao Song, Jian Zhao, Haibin Shi, Ruibin Li, Yangyun Wang & Leshuai W. Zhang

To cite this article: Yongming Liu, Huan Yu, Xihui Zhang, Yong Wang, Zhentao Song, Jian Zhao, Haibin Shi, Ruibin Li, Yangyun Wang & Leshuai W. Zhang (2018) The protective role of autophagy in nephrotoxicity induced by bismuth nanoparticles through AMPK/mTOR pathway, *Nanotoxicology*, 12:6, 586-601, DOI: [10.1080/17435390.2018.1466932](https://doi.org/10.1080/17435390.2018.1466932)

To link to this article: <https://doi.org/10.1080/17435390.2018.1466932>



[View supplementary material](#) 



Published online: 06 May 2018.



[Submit your article to this journal](#) 



Article views: 168



[View Crossmark data](#) 



Citing articles: 1 [View citing articles](#) 

ARTICLE



The protective role of autophagy in nephrotoxicity induced by bismuth nanoparticles through AMPK/mTOR pathway

Yongming Liu^{a*}, Huan Yu^{a*}, Xihui Zhang^a, Yong Wang^a, Zhentao Song^b, Jian Zhao^b, Haibin Shi^a, Ruibin Li^a, Yangyun Wang^a and Leshuai W. Zhang^a

^aSchool for Radiological and Interdisciplinary Sciences (RAD-X), State Key Laboratory of Radiation Medicine and Protection, School of Radiation Medicine and Protection, and Collaborative Innovation Center of Radiation Medicine of Jiangsu Higher Education Institutions, Soochow University, Suzhou, PR China; ^bState Key Laboratory of Bioreactor Engineering, East China University of Science and Technology, Shanghai, PR China

ABSTRACT

Bismuth is widely used in metallurgy, cosmetic industry, and medical diagnosis and recently, bismuth nanoparticles (NPs) (BiNP) have been made and proved to be excellent CT imaging agents. Previously, we have synthesized bovine serum albumin based BiNP for imaging purpose but we found a temporary kidney injury by BiNP. Due to the reported adverse events of bismuth on human health, we extended our studies on the mechanisms for BiNP induced nephrotoxicity. Blood biochemical analysis indicated the increase in creatinine (CREA) and blood urea nitrogen (BUN), and intraluminal cast formation with cell apoptosis/necrosis was evident in proximal convoluted tubules (PCTs) of mice. BiNP induced acute kidney injury (AKI) was associated with an increase in LC3II, while the autophagic flux indicator p62 remained unchanged. Chloroquine and rapamycin were used to evaluate the role of autophagy in AKI caused by BiNP. Results showed that BiNP induced AKI was further attenuated by rapamycin, while AKI became severe when chloroquine was applied. *In vitro* studies further proved BiNP induced autophagy in human embryonic kidney cells 293, presented as autophagic vacuole (AV) formation along with increased levels of autophagy-related proteins including LC3II, Beclin1, and Atg12. Specifically, reactive oxygen species (ROS) generated by BiNP could be the major inducer of autophagy, because ROS blockage attenuated autophagy. Autophagy induced by BiNP was primarily regulated by AMPK/mTOR signal pathway and partially regulated by Akt/mTOR. Our study provides fundamental theory to better understand bismuth induced nephrotoxicity for better clinical application of bismuth related compounds.

ARTICLE HISTORY

Received 6 February 2018

Revised 13 April 2018

Accepted 16 April 2018

KEYWORDS

Bismuth; CT imaging; acute kidney injury; autophagy; cell signaling pathway

Introduction

With the development of nanotechnology and material science, a numerous of engineered nanomaterials have been widely applied in our daily lives. Owing to the specific physicochemical properties of nanomaterials, nanotechnology was considered as an attractive strategy for cancer therapies and diagnostics (Caracciolo et al. 2013; Park et al. 2013; Taratula et al. 2013). Some nanomaterials containing elements with high atomic numbers, for example, gold, iodine, bismuth, and rare earth elements, have been proved to be excellent radiosensitizers (Jain et al. 2011; Joh et al. 2013; Xiao et al. 2013; Zhang et al. 2014a, 2014b; Song et al. 2016). Compared to traditional

contrast agents, novel CT contrast agents are emerging to improve the resolution and specificity of the targets for diagnosis in order to effectively track and confirm the diseased localization in organs. The above-mentioned nanomaterials usually possess as X-ray computed tomography (CT) contrast agents potentials for tumor imaging (Ferrari 2005; Gupta and Gupta 2005).

In recent years, bismuth-based nanomaterials have been demonstrated to be superior to iodinated CT contrast agents, owing to their high X-ray attenuation capability, long residence time and minimal residues in the organism (Kinsella et al. 2011; Li et al. 2013; Zhang et al. 2014b). Different bismuth

CONTACT Yangyun Wang  yywang578@suda.edu.cn; Leshuai W. Zhang  zhangls@suda.edu.cn  College of Radiation Medicine and Protection, Soochow University, 199 Renai Rd, Suzhou 215123, Jiangsu Province, PR China

 Supplemental data for this article can be accessed [here](#).

*These authors contributed equally to this work.

© 2018 Informa UK Limited, trading as Taylor & Francis Group

sulfide nanoparticles (NPs) were prepared and applied for tumor-targeted therapy and multimodal imaging. For example, bismuth sulfide nanorods possess excellent photothermal effects with enhanced contrast in CT imaging. These combined features endow bismuth NP with functions of precise visual guide on tumor localization and tumors destruction (Liu et al. 2016b). In our previous work, we found that bismuth sulfide NP (BiNP) can serve as an excellent contrast agent for CT imaging owing to its broad X-ray absorption feature (Wang et al. 2016). In addition, other studies showed that bismuth sulfide nanorods can potentiate the anti-tumor efficacy of radiotherapy as radiosensitizers (Cheng et al. 2017). Other than bismuth sulfide NP, functionalized bismuth oxide nanomaterials can also be used as contrast agents, which have exhibited excellent solubility and biocompatibility. For example, hyaluronic acid-functionalized bismuth oxide NP was found to enhance CT imaging of tumor with enhanced radiosensitization (Du et al. 2017). Therefore, other than traditional iodinated or gold-based systems, bismuth nanomaterials may be used as alternative CT contrast agents.

However, the potential applications of bismuth nanomaterials suggest the exposure and risk of bismuth on human and environmental health. Other than bismuth nanomaterials, bismuth salts such as colloidal bismuth subcitrate (CBS) and bismuth subsalicylate have been commonly used to treat peptic ulcers (Andrews et al. 2006; Marcus, Sachs, and Scott 2015). In addition, bismuth compounds such as bismuth vanadate, bismuth nitrate, and bismuth oxychloride have been applied as the raw materials for foundation in cosmetics. However, overdose of bismuth compounds can cause acute renal failure that has been mentioned by a numerous of clinical cases (Islek et al. 2001). For example, during the treatment of *Helicobacter pylori* infections, CBS overdose has been reported to result in severe nephrotoxicity, such as necrosis in the proximal tubules (Leussink et al. 2001). In addition, bismuth oxybromide (BiOBr) NPs have been utilized in semiconductor industry, but BiOBr was found to be toxic to human skin keratinocytes (Gao et al. 2015). In spite of plenty case reports on bismuth nephrotoxicity, there were very limited studies to elucidate the mechanisms of bismuth nephrotoxicity in the cellular and molecular level.

During the past one decade, autophagy has been used for exploration on the mechanisms of neurodegeneration, cardiovascular disease, and cancer therapy (Lavandero et al. 2013; Frake et al. 2015; White 2015). In addition, several toxic heavy metals such as cadmium and iron oxide have been found to induce autophagy in the kidney (Chargui et al. 2011; Šebeková et al. 2014). Autophagy is a typical physiological adaptation of the cells with the microenvironment, which includes initiation, vesicle nucleation, vesicle elongation, fusion for protein degradation, and termination (Kim and Lee 2014; Tanida 2011). However, under severe pathological conditions, autophagy may result in cell death (Wu et al. 2009; Sutton et al. 2018). Many heavy metals have been found to elicit autophagy, which was demonstrated to play a protective role in metal toxicity (Liu et al. 2016a). In addition, some nanomaterials also introduce autophagy, such as silica, tantalum, and gold NP (Ma et al. 2011; Guo et al. 2016; Kang et al. 2017). Unlike other heavy metals, bismuth possesses moderate toxicity while the mechanism remains unknown. Recently we found different bismuth compounds can induce autophagy, we expect that bismuth nanoform may have similar effects (Liu et al. 2017).

In this work, we evaluated the toxicity of bismuth NP synthesized from bismuth nitrate and bovine serum albumin, and we found kidney injury with the occurrence of autophagy. Therefore, it became our interest to elucidate the role of autophagy and associated or related signaling pathway during bismuth NP induced acute kidney injury (AKI), which can help us understand the mechanisms of bismuth induced nephrotoxicity.

Methods and materials

Chemicals and materials

Dulbecco's modified eagle medium (DMEM) and fetal bovine serum (FBS) were purchased from Thermo Fisher Scientific (Waltham, MA). All antibodies for LC3B (#2775S), p62 (#5114S), Atg5 (#12994S), Atg12 (#4180S), Beclin1 (#3495S), GAPDH, AMPK (#5831T), p-AMPK (Thr172) (#2535T), PI3K (#4257T), p-PI3K (Ser249) (#13857S), Akt (#4691T), p-Akt (Ser473) (#4060T), MAPK (#4695T), p-MAPK (Thr202) (#4370T), mTOR (#2983S), and p-mTOR (Ser2448) (#5536S) were purchased from Cell Signaling

Technology (Danvers, MA). The fluorescent probe 2',7'-dichlorofluorescein diacetate (DCFH-DA), radio-immunoprecipitation assay (RIPA) buffer, and bicinchoninic acid (BCA) protein assay kit were acquired from Beyotime (Shanghai, China). *N*-acetylcysteine (NAC) and monodansylcadaverine (MDC) were purchased from Sigma-Aldrich (St. Louis, MO). Lipofectamine 2000 was obtained from Life Technologies (Carlsbad, CA). Osmium tetroxide was purchased from Zhongjingkeyi Technology Co. Ltd (Nanjing, China). Tachyplesus amebocyte lysate (TAL) was purchased from Xiamen Bioendo Technology Co. Ltd (Xiamen, China).

Cell culture

Human embryonic kidney 293 (HEK293) cell line was purchased from Cell Bank of Chinese Academy of Sciences (Shanghai, China). Cells were cultured in DMEM supplemented with 10% of FBS and 0.5% penicillin-streptomycin solution, and maintained at 37 °C and 95% air/5% CO₂.

BiNP synthesis and characterization

In our previous work, we have made BiNP synthesized from bismuth nitrate and BSA, showing excellent CT contrast ability (Wang 2016; Liu et al. 2017). In brief, BSA was incubated with bismuth nitrate in the acidic environment (pH < 5) to have bismuth ion bound to its functional groups. The pH of the solution was adjusted to 12 using 2 M NaOH. Sulfide ions were then released from BSA in basic environment and the solution was changed to dark black color, indicating BiNP formation. BiNP was observed by transmission electron microscope (TEM, Tecnai G2 Spirit BioTWIN, FEI, Hillsboro, OR). For negative staining, BiNP solution was dropped onto a formvar-coated grid and 0.5% uranyl acetate solution was applied to the sample for 1 min, followed by the removal of the staining solution using filter paper and observation by TEM. In addition, the hydrodynamic diameters and surface charge of BiNP in different solvent (Water, PBS, and DMEM) were measured using Zetasizer Nano ZS90 (Malvern, Worcestershire, UK) and the absorbance of the spectra of BiNP was analyzed by UV-vis spectrum ranging from 250 to 1000 nm.

Western blot for protein analysis

HEK293 cells were seeded into 6-well plates at concentration of 1.5×10^5 /ml and treated with BiNP for 24 h. Cells were trypsinized and lysed in RIPA buffer. Supernatant was collected by centrifugation at 14 000 rpm at 4 °C for 10 min. Protein concentrations were determined using the BCA assay (Beyotime, Shanghai, China) and protein (30 g) were loaded on 15% polyacrylamide gel and subjected to electrophoresis. Protein bands were transferred onto nitrocellulose membranes, which were blocked in TBST (0.1% Tween-20) containing 5% fat-free milk or 3% bovine serum albumin (for phosphorylated protein) for 1 h at room temperature. Membranes were further incubated with primary antibodies (the concentration of each antibody was according to manufacturer's instruction) overnight at 4 °C and washed with TBST three times. After incubation with secondary peroxidase-conjugated anti-rabbit IgG for 1 h, the membranes were washed three times and the protein bands were detected by enhanced chemiluminescence detection system (Thermo Fisher Scientific, Waltham, MA) to determine the protein expression.

Ultrastructural observation of autophagy in TEM

Cells were incubated with BiNP for 24 h, trypsinized for 1 min and collected, washed with 0.1 M phosphate buffer for two times and pre-embedded in 3% low melting agarose. Fixation of cells was conducted in Trump's fixative for 1 h at 4 °C, rinsed with 0.1 M phosphate buffer for three times and post-fixed with 1% osmium tetroxide for 1 h. Samples were dehydrated through 50, 70, 95, and 100% ethanol, replaced with acetone, infiltrated and embedded with Spurr's resin (Rusmar Foam Technologies, West Chester, PA). Thin sections at 80 nm were cut using an ultramicrotome (Leica EM UC7, Leica Microsystems, Wetzlar, Germany), stained with lead citrate and uranyl acetate, and placed on 200 mesh copper grids and imaged on TEM operating at an accelerating voltage of 120 kV.

Monodansylcadaverine staining

MDC is an *in vitro* marker for autophagic vacuoles (AV) (Munafó and Colombo 2001). Cells were seeded in 35 mm confocal dish at concentration of

1.5×10^5 /ml and cultured in DMEM supplemented with 10% FBS overnight. Cells were pretreated with 0.5 mM NAC, a known ROS scavenger, and incubated with BiNP for 24 h. Cells were washed with PBS for three times and labeled with 50 nM MDC at 37 °C for 30 min in the dark. Subsequently, cells were washed twice with PBS and immediately visualized and imaged by confocal laser scanning microscopy (CLSM) at excitation wavelength at 380 nm and emission peak at 530 nm using Olympus FV1200, FV10-ASW 4.2 software (Olympus Corporation, Tokyo, Japan).

Detection of intracellular reactive oxygen species

Measurement of intracellular reactive oxygen species (ROS) was performed by quantification of the fluorescence intensity of 2,7-dichlorofluorescein (DCF). Cells were seeded in 35 mm confocal dish at the concentration of 1.5×10^5 /ml and cultured in DMEM supplemented with 10% FBS overnight. Cells were treated with different concentrations of BiNP for 24 h and stained with 10 μ M DCFH-DA for 30 min at 37 °C in the dark. Cells were washed twice with PBS and imaged using CLSM 488 ex/525 em, and fluorescence intensity was analyzed by ImageJ software (Image J System, Bethesda, MD).

GFP-LC3 plasmid transient transfection

The eukaryotic expression plasmid EGFP-LC3b-pCMV (Miaolingbio, Wuhan, China) was transfected into HEK293 cells using Lipofectamine 2000 (Invitrogen, Carlsbad, CA) according to manufacturer's instruction. After 12 h of transfection, cells were visualized in fluorescence microscopy to determine the transfection efficiency. Cells were further incubated with different concentrations of BiNP for additional 24 h and GFP-LC3B positive cells were imaged using CLSM.

Animal experiments

Female Balb/c mice with ages of five weeks were purchased from Cavens Laboratory Animal Company (Changzhou, China). Mice were kept in 23 ± 2 °C laboratory conditions and were approved by the Animal Ethics Committee of Soochow University. Mice were randomly allotted into different groups. In one experiment set, four groups of mice (six for each

group) were injected with PBS or BiNP at 1.25, 2.5, and 5 mg/kg, respectively. In another experiment, four groups of mice were injected with PBS (IV) or 2.5 mg/kg BiNP (IV), 2.5 mg/kg BiNP (IV) with 3 mg/kg rapamycin pretreatment (IP, 1 h before BiNP injection), 2.5 mg/kg BiNP (IV) and 60 mg/kg chloroquine pretreatment (IP, 1 h before BiNP injection). Mice were sacrificed for necropsy three days later. Mice were anesthetized with pentobarbital, and blood samples were obtained by cardiac puncture using syringes containing EDTA followed by centrifugation for serum collection. Total protein, blood urea nitrogen (BUN), creatinine (CREA), sodium, potassium, and chloride were determined. For protein expression analysis, left kidney tissue was collected and lysed in RIPA buffer containing protease inhibitors and other chemical inhibitors, followed by western blot detection.

Histopathological observation of kidney

The right kidney of each mouse was fixed with 4% paraformaldehyde, dehydrated, and embedded with paraffin. The sample was sectioned at 5 μ m and stained with standard Hematoxylin&Eosin (H&E) staining procedure. Slides were examined and imaged under light microscopy.

Immunohistochemistry staining

Paraffin-embedded tissue sections were deparaffinized, rehydrated, and high-pressure steamed in sodium citrate buffer at pH 6.0 for antigen retrieval. Slides were immersed in 3% hydrogen peroxide for 10 min to block the activity of endogenous peroxidase. Tissue sections were incubated overnight at 4 °C with LC3B Rabbit mAb (Cell Signaling Technology, Danvers, MA, 1:200) and incubated with anti-rabbit biotinylated secondary antibody for 20 min at 37 °C. Slides were developed using HRP-labeled streptavidin and DAB (Histostain-Plus Kit, FCMACS, Nanjing, China) and counterstained with hematoxylin staining. Immunohistochemical staining sections were analyzed by light microscopy.

Statistical analysis

All data were expressed as mean \pm SE. The significance of difference between mean values was analyzed by

one-way ANOVA and a probability value of $p < 0.05$ was considered statistically significant.

Results

Characterization of BiNP

The preparation of BiNP solution can be found from our previous work (Wang et al. 2016). BiNP solution was dialyzed to remove bismuth residues during synthesis. First, endotoxin of BiNP solution was tested using gel clot TAL assay and the process was according to manufacturer's instruction. The result showed that the LPS in the BiNP suspension is lower than 0.25 EU/ml. BiNP observed in TEM exhibited a spherical shape and the sizes of BiNP were 6–7 nm (Figure 1(A)). Negative staining of BiNP indicated slightly smaller sizes than those observed in normal mode of TEM (Figure 1(B)). UV-vis spectra did not show any distinct absorbance peak for BiNP suspension (Figure 1(C)). The hydrodynamic sizes were evaluated by dynamic light scattering (DLS). BiNP showed an average size of 63.72 nm in water, while the size of BiNP was reduced to 52.46 and 52.92 in PBS and DMEM, respectively (Table 1). Surface charge of BiNP in water was -27.43 mV, while the charge value was reduced to -10.71 and -11.38 mV in PBS and DMEM, respectively (Table 2). In addition, BiNP has been demonstrated with excellent CT contrast ability and can be used as a potential contrast agent. However, we observed a transient nephrotoxicity induced by BiNP with unidentified mechanisms, which is the focus of this work.

Bismuth induced biochemical and pathological changes

Mice were intravenously injected with BiNP for three days and serum was collected for blood biochemical analysis. Total protein, BUN, CREA, sodium, potassium, and chloride were measured and the results were presented in Figure 2 and Figure S1. Compared to control group, increases of CREA, BUN, and total protein by BiNP were evident in a dose-dependent manner (Figure 2). No changes in sodium and chloride between the control and the BiNP treated group were found, while a slight increase in potassium was observed with elevated BiNP concentrations (Figure S1). Therefore, the above results suggested

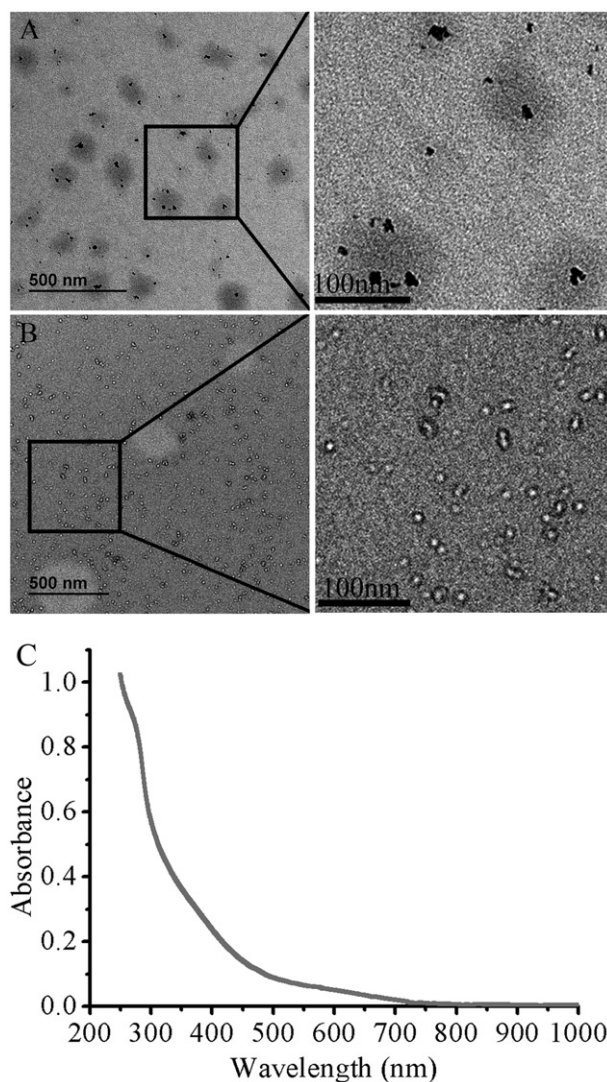


Figure 1. Characterization of BiNP. (A) BiNP in transmission electron microscopy. (B) Negative staining of BiNP using uranyl acetate solution. (C) Absorbance spectra of BiNP.

Table 1. Hydrodynamic sizes of BiNP.

Solution	Water	PBS	DMEM
$\bar{x} \pm SE$ (nm)	63.72 ± 0.71	52.46 ± 0.3	52.92 ± 0.91

Values are presented as the mean \pm SE.

Table 2. Surface charges of BiNP.

Solution	Water	PBS	DMEM
$\bar{x} \pm SE$ (mV)	-27.43 ± 0.39	-10.71 ± 0.53	-11.38 ± 0.5

Values are presented as the mean \pm SE.

that BiNP may cause AKI, which required further observation in H&E staining.

In order to confirm that BiNP can induce AKI, heart, kidney, lung, liver, and spleen were collected for pathological evaluation. The results showed in Figure 3 indicated the kidney injury by BiNP. Normal proximal convoluted tubules (PCTs) were

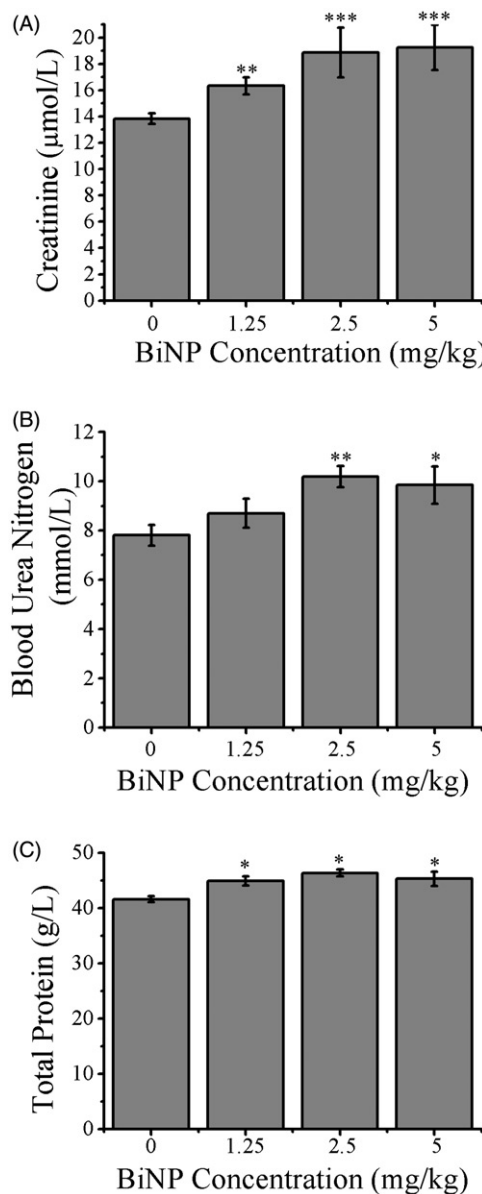


Figure 2. Routine biochemical test of blood intravenously injected with BiNP. Mice were injected with BiNP at 1.25, 2.5, and 5 mg/kg or PBS for three days and serum were collected for biochemical test. (A) creatinine; (B) blood urea nitrogen; and (C) total protein.

presented in PBS treated group, while apoptotic cells with condensed nuclei in PCT were frequently observed in BiNP treated individuals at 1.25 mg/kg (black arrows in Figure 3(B)). Kidney injury was gradually exacerbated in the group dosed with 2.5 mg/kg BiNP, represented by the occurrence of necrotic cells (arrowheads, Figure 3(C)) other than apoptotic cells in PCT. Kidney injury became severe at the highest dose group (5 mg/kg), in which the necrosis of the ruptured epithelial cells lining in renal tubules and intraluminal cast formation were evident (stars, Figure 3(D)). As the result, H&E stained

sections showed the AKI by BiNP in a dose-dependent manner. Other than kidney, no significant pathological changes in other major organs such as liver, heart, lung, and spleen were found, indicating that the injury of BiNP was tissue specific.

BiNP induced autophagy in kidney

Microtubule-associated protein light chain 3 (LC3) is well recognized to monitor autophagy, during which the cytosolic LC3I is modified by phosphatidylethanolamine to form membrane bound LC3II (Duan et al. 2014; Kim and Lee 2014). To study if autophagy occurs during BiNP induced AKI, LC3I/II protein was evaluated by western blotting (Figure 4). BiNP at 1.25, 2.5, and 5 mg/kg all resulted in a significant increase in both LC3I and LC3II in mouse kidney.

LC3II may be accumulated due to either autophagy induction or impairment of autophagic flux. To further investigate the mechanisms of autophagy induced by BiNP, we quantified p62 (SQSTM1/sequestome1), a specific substrate that can be degraded by regular autophagy flux (Pankiv et al. 2007). BiNP did not alter the protein expression of p62, demonstrating that autophagic flux was not blocked by NPs. We can draw a conclusion that BiNP is the initiator of autophagy and did not block autophagic flux during the process of kidney injury.

The protective role of autophagy on AKI by BiNP

Although BiNP was proved to induce autophagy in kidney, it remained unknown if autophagy contributed to kidney injury by BiNP, or oppositely, played a protective role during BiNP treatment. Here, rapamycin or chloroquine was used to induce autophagy or block autophagic flux, respectively, in 2.5 mg/kg BiNP treated mice. As shown in Figure 5(A,B), BiNP introduced an increase in CREA and BUN, similar as Figure 2. Chloroquine has been demonstrated to inhibit the fusion between autophagosome and lysosome, preventing the formation of autolysosome and consequently, the autophagic flux blockage (Kawai et al. 2007; Ma et al. 2012; Cui et al. 2017). The use of chloroquine further increased the level of CREA and BUN compared to BiNP treatment alone. In comparison, additional autophagy induction by rapamycin alleviated BiNP induced nephrotoxicity, identified by

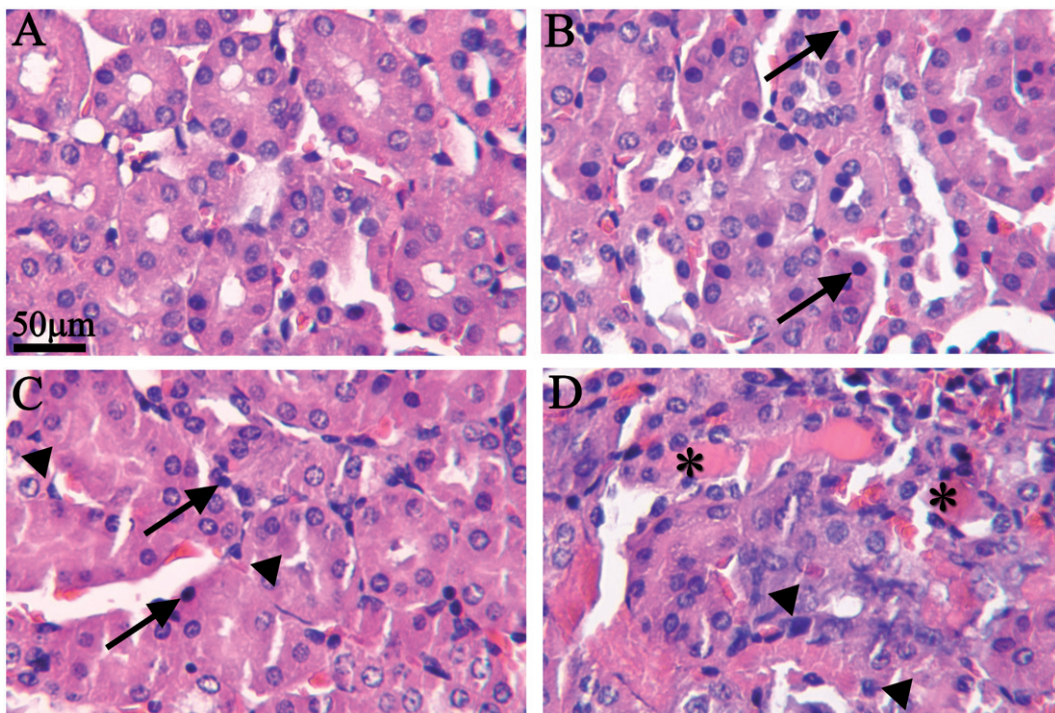


Figure 3. H&E staining showing BiNP induced kidney injury. Mice were injected with BiNP for three days and kidneys were collected for H&E staining and microscopic observation. (A) PBS as the control; (B) 1.25 mg/kg BiNP; (C) 2.5 mg/kg BiNP; (D) 5 mg/kg BiNP. Black arrow indicates apoptotic cells, arrowhead is for necrotic cells, and star symbol represents the cast in the renal tubules.

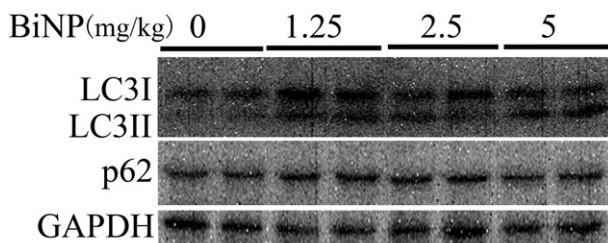


Figure 4. BiNP induced autophagy in kidney tissue. Mice were injected with BiNP at different doses for three days and kidney were harvested, sonicated, and solubilized for western blot evaluation. Autophagy-related markers were detected by western blot using LC3I/II and p62 mAbs. GAPDH was used as the loading control.

elevated CREA and BUN. Therefore, very likely autophagy played a protective role in BiNP induced nephrotoxicity based on blood biochemical analysis.

Immunohistochemical and H&E staining confirmed the role of autophagy during BiNP induced AKI when chloroquine and rapamycin were further applied. As shown in Figure 5(C), BiNP alone induced a moderate level of autophagy, demonstrated by increased LC3-positive puncta, or a slight increase of brown color in the proximal tubule cells. Chloroquine as a blocker for autophagic flux further increased LC3 expression. Rapamycin also increased LC3 expression as a classical inducer for autophagy

(Figure 5(C)). From H&E point of view, pale-staining of hematoxylin indicates renal tubule necrosis by BiNP, characterized as cell swelling, fragmented cytoplasm, and cytoplasmic vacuolization (arrows). In addition, interstitial inflammatory infiltration was evident (arrowheads in Figure 5(D)). Compared to BiNP treatment alone, BiNP combination with chloroquine exacerbated the kidney damage, identified by granular casts (necrotic cell debris) and cellular sloughing. In contrast, the application of rapamycin attenuated BiNP induced nephrotoxicity that was characterized by reduced pale staining of hematoxylin, indicating the attenuation of kidney injury due to the further induction of autophagy by rapamycin (Figure 5(D)).

BiNP induced autophagy in HEK293 cells

To initiate the mechanistic studies of autophagy induced by BiNP, HEK293 cell line, a type of embryonic kidney cell line was used for *in vitro* experiments. TEM is considered as the gold standard method to determine the occurrence of autophagy, characterized as the formation of double-membrane based vacuoles. HEK293 cells were treated with

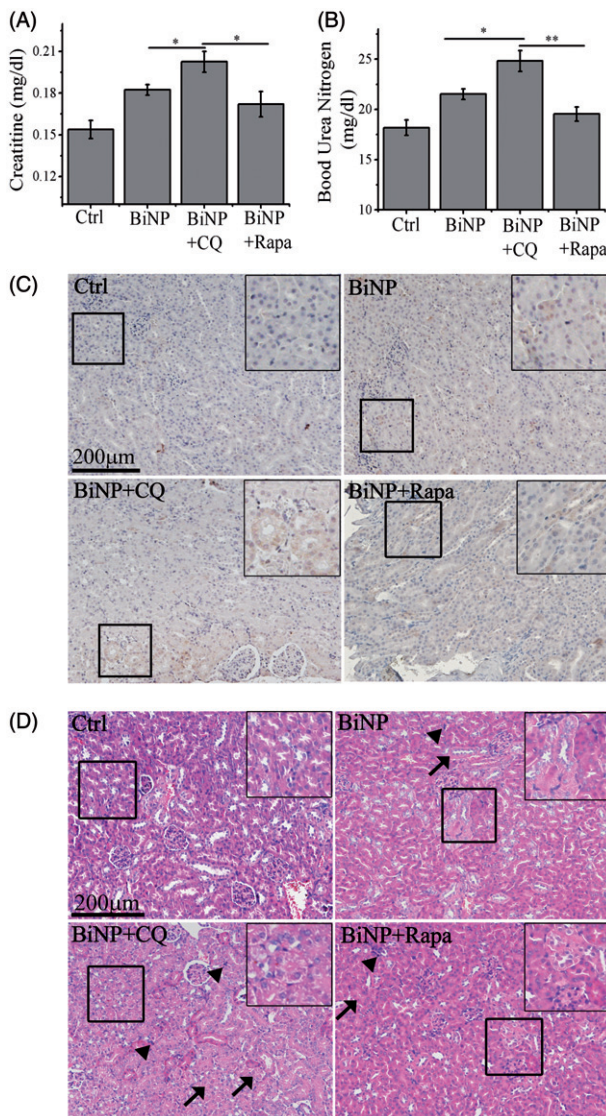


Figure 5. The role of autophagy in BiNP induced kidney injury based on blood biochemical tests and pathological observations. Mice were pre-injected with PBS, 3 mg/kg rapamycin, and 60 mg/kg chloroquine for 1 h, followed by the injection of 2.5 mg/kg BiNP for three days. (A) Serum creatinine and (B) blood urea nitrogen (BUN). All data represent means \pm SE from three independent experiments. * p < 0.05, ** p < 0.01. (C) Immunohistochemistry staining of LC3 of kidney tissue sections. (D) H&E staining of kidney. Intact proximal tubules are available in control group, while BiNP treated group showed renal tubule necrosis and fragmented and vacuolized cytoplasm, indicated as pale hematoxylin staining (arrows). Cell injury by necrosis and vacuolization became more evident in BiNP + CQ group, along with interstitial inflammatory infiltration (arrowheads), while rapamycin alleviated BiNP induced nephrotoxicity with less pale hematoxylin staining. CQ: chloroquine; Rapa: rapamycin.

BiNP for 24 h, dehydrated, embedded in Spurr's resin and observed for ultrastructural characteristics of autophagy in TEM. As shown in Figure 6(A), non-treated cells are morphologically normal, identified

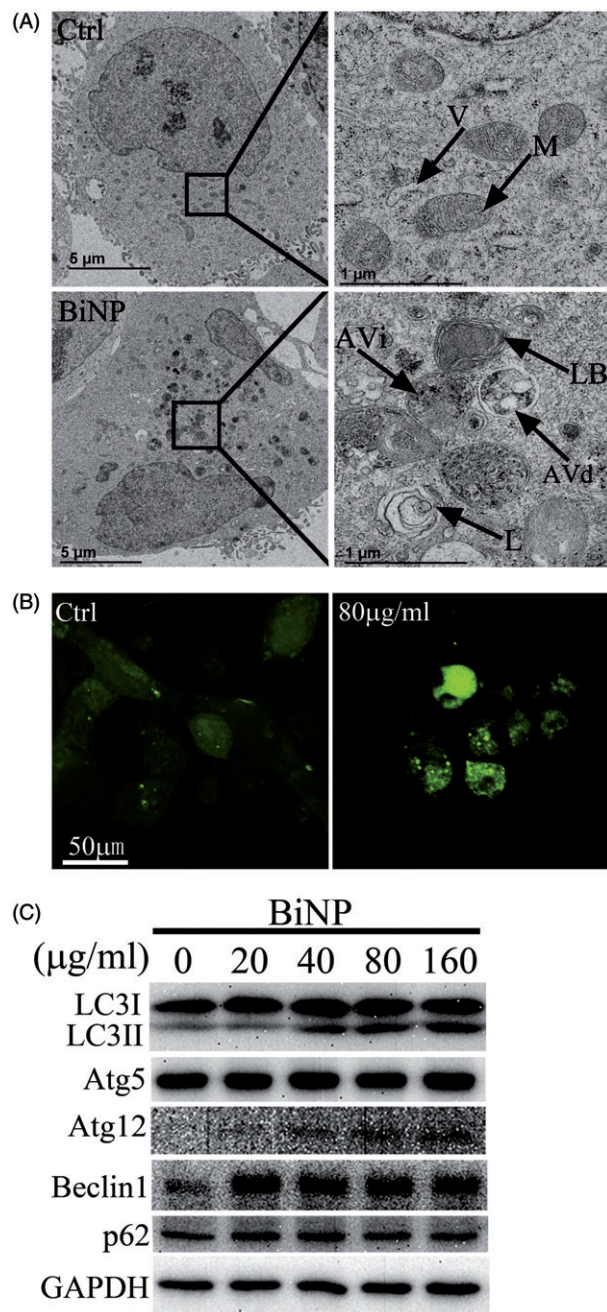


Figure 6. BiNP is capable of autophagy induction *in vitro*. (A) Intracellular autophagy observation by TEM. HEK293 Cells were treated with 80 μ g/ml BiNP for 24 h, subjected to dehydration, resin embedding and sectioning. Non-treated cells (control) showed healthy mitochondria (M) and translucent intracellular vesicles (V). Treated cells showed autophagy presented by the initial autophagic vacuoles (AVi) and degradative autophagic vacuole (AVd). Lamellar bodies (LB) and normal lysosomes (L) are also commonly found. (B) Autophagy induction in HEK293 cells with GFP-LC3 overexpression. HEK293 cells were transfected with GFP-LC3 plasmid and exposed with 80 μ g/ml BiNP for 24 h. The punctate pattern of GFP-LC3 in BiNP treated cells were found by CLSM, while non-treated cells showed a diffused cytoplasmic distribution of LC3. (C) BiNP modulated the expression of a series of autophagy-related proteins. Cells were treated with different concentrations of BiNP up to 160 μ g/ml for 24 h and expression of LC3, Atg5, Atg12, Beclin 1 and p62 were detected by western blot.

with translucent vacuoles (V) as well as intact mitochondria (M). In comparison, HEK293 cells exposed to BiNP exhibited typical double membrane based vacuoles, namely, initial AV (AVi), in which the cytoplasmic contents ready for degradation were evident. In addition, degradative AV (AVd), or autolysosomes were detected. Other than autophagosomes and autolysosomes, typical lysosomes (L) and lamellar bodies (LB) filled with phospholipids can be identified (Figure 6(A)).

The occurrence of autophagy by BiNP can be also verified by the formation of green puncta in GFP-LC3 overexpressing cells. Historically, cells containing more than three GFP-LC3 puncta were defined as autophagy-positive cells (Pedro et al. 2016). HEK293 cells were transfected with GFP-LC3 plasmids followed by incubation with BiNP for 24 h and observed in CLSM. Cells with a numerous of intracellular GFP-LC3 puncta were found in BiNP treated sample, while homogenously distributed LC3 in the cytoplasm was found in non-treated cells (Figure 6(B)). Therefore, our observation in GFP-LC3 overexpressing cells demonstrated that BiNP were capable of inducing autophagy *in vitro*.

To investigate the regulation of other autophagy-related proteins by BiNP, HEK293 cells were incubated with different concentrations of BiNP and collected for western blot analysis. We found a dose-dependent increase of LC3II by BiNP. Other than LC3, Beclin1 and Atg12 were also significantly increased compared to control. In comparison, Atg5 that can form complex with Atg12, did not show any changes when cells were treated with BiNP (Figure 6(C)). Finally, p62 as the marker for autophagic flux inhibition did not change by BiNP, confirming again that BiNP is only the autophagy inducer instead of the autophagic flux blocker, which is in accordance with *in vivo* data presented in Figure 4.

AMPK/mTOR signal pathway was involved in autophagy induction by BiNP

To elucidate the molecular mechanism or cell signaling pathway BiNP utilized for autophagy induction, we performed immunoblot to examine phosphorylation status of AMPK, PI3K, Akt, MAPK, and mTOR *in vitro*. HEK293 cells were treated with 80 µg/ml BiNP at different time points, and collected for western blot analysis. The result showed that

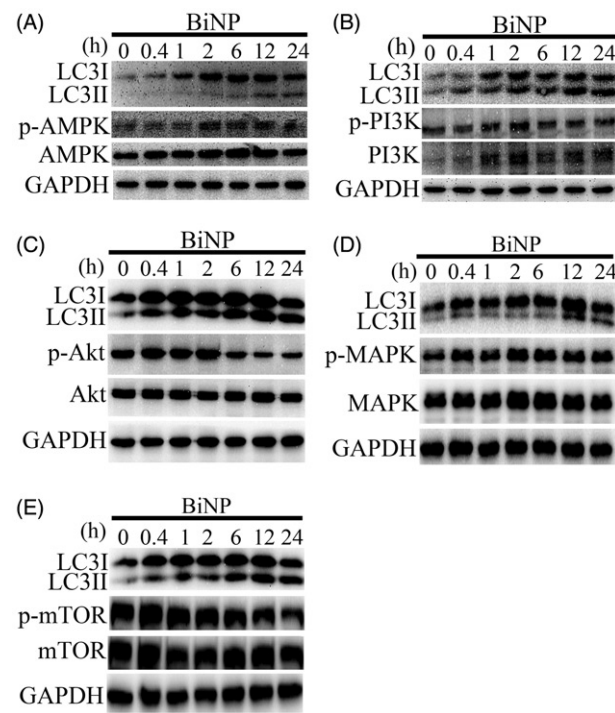


Figure 7. AMPK/mTOR signal pathway was involved in autophagy induction by BiNP. HEK293 cells were incubated with 80 µg/ml BiNP at 0, 0.4, 1, 2, 6, 12, and 24 h. Cells were subjected with SDS-PAGE and upstream proteins of autophagy were detected by western blot. (A) LC3, p-AMPK and total AMPK expression; (B) LC3, p-PI3K and total PI3K expression; (C) LC3, p-Akt and total Akt expression; (D) LC3, p-MAPK and total MAPK expression; (E) LC3, p-mTOR and total mTOR expression.

phosphorylation of AMPK (p-AMPK) was significantly increased with time (Figure 7(A)). In the meanwhile, p-mTOR was significantly decreased in a time-dependent manner (Figure 7(E)). Although p-Akt was evidently decreased, its upstream protein PI3K had no change in phosphorylation compared to the control sample (Figure 7(B,C)). In contrast, p-MAPK and total MAPK did not show any changes (Figure 7(D)). Overall, our results indicated that autophagy induced by BiNP was mainly regulated by AMPK/mTOR and partially regulated by Akt/mTOR signaling pathways.

Effects of reactive oxygen species on BiNP induced autophagy

A numerous of literature have suggested that ROS are classical autophagy inducers (Scherz-Shouval, Shvets, and Elazar 2007; Azad, Chen, and Gibson 2009; Lee, Giordano, and Zhang 2012; Lavallard et al. 2012; Wang et al. 2015). Therefore, we

measured ROS level using DCFH-DA probe. Our results showed the weak green fluorescence in untreated cells, while intracellular mean fluorescence intensity (MFI) significantly increased in a dose-dependent manner when cells were treated with BiNP (Figure 8(A)). MFI was calculated by ImageJ software (Image J System, Bethesda, MD) and plotted as in Figure 8(B). We also measured the ROS levels using flow cytometry, and obtained similar results (Figure 8(C)). These results all suggested that BiNP can induce ROS production.

To investigate the role of ROS on BiNP induced autophagy, HEK293 cells were treated with BiNP with/without NAC for 24 h. ROS scavenger NAC can efficiently block ROS generation caused by BiNP in HEK293 cells (Figure 9(A)). These cells were stained with MDC to detect AVs. As shown in Figure 9(B), weak MDC fluorescence was detected in the control cells, while MDC fluorescence was significantly increased in BiNP treatment cells. However, when cells were co-treated with BiNP and NAC, MDC fluorescence was significantly reduced compared to BiNP treatment alone, which was quantified by intracellular fluorescence analysis in ImageJ software (Image J System, Bethesda, MD) (Figure 9(C)). In order to confirm autophagy by BiNP was reduced when ROS was inhibited by NAC, LC3 protein level was analyzed by western blot. HEK293 cells were treated with BiNP with/without NAC for 24 h. The result showed that LC3II protein level increased by BiNP was attenuated by NAC (Figure 9(D)). Therefore, these results indicated that ROS is the initiator of autophagy caused by BiNP.

Discussion

Nanomaterials containing bismuth have been developed for CT imaging, photothermal therapy, and drug delivery (Chen et al. 2015; Li et al. 2016). In addition, bismuth compounds can be used in medical applications. For example, CBS and bismuth subsalicylate are commonly used in *H. pylori* treatment regimens. However, other studies found that overdose of CBS induced cell death and result in nephrotoxicity (Leussink et al. 2001; Marcus, Sachs, and Scott 2015). In our previous work, we prepared ultrasmall BiNP and its ultrastructure is shown in Figure 1. We found a reversible nephrotoxicity after the intravenous injection of BiNP, indicated by the

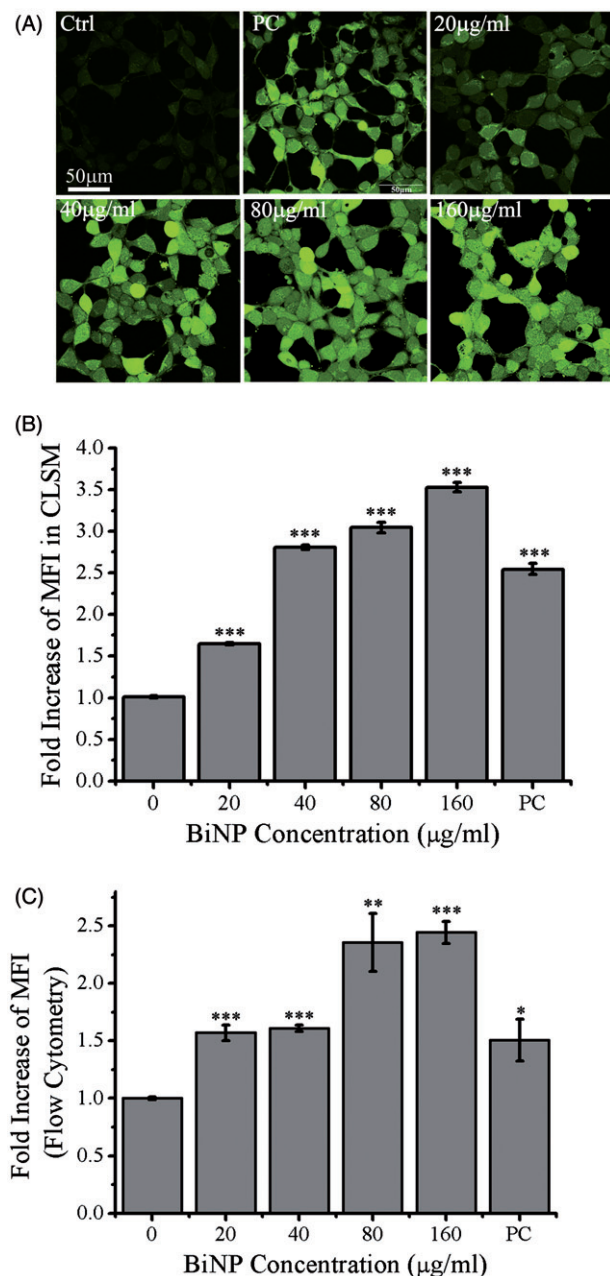


Figure 8. BiNP induces the generation of intracellular reactive oxygen species (ROS). HEK293 cells were treated with different concentrations of BiNP for 24 h. (A) Intracellular ROS production was stained with DCFH-DA and observed by CLSM. Ctrl represents negative control and PC indicates positive control (Rosup in the assay kit) (B) ROS fluorescence intensity in CLSM quantified by ImageJ. (C) Intracellular ROS produced relative to control were measured using flow cytometry. All data represents means $\pm \text{SE}$ from three independent experiments. * $p < 0.05$, ** $p < 0.01$, *** $p < 0.001$.

temporary increase in serum CREA and BUN (Wang et al. 2016). In this study, we extended our research for BiNP induced kidney injury, emphasizing on the role of autophagy and associated cell signaling pathways in nephrotoxicity.

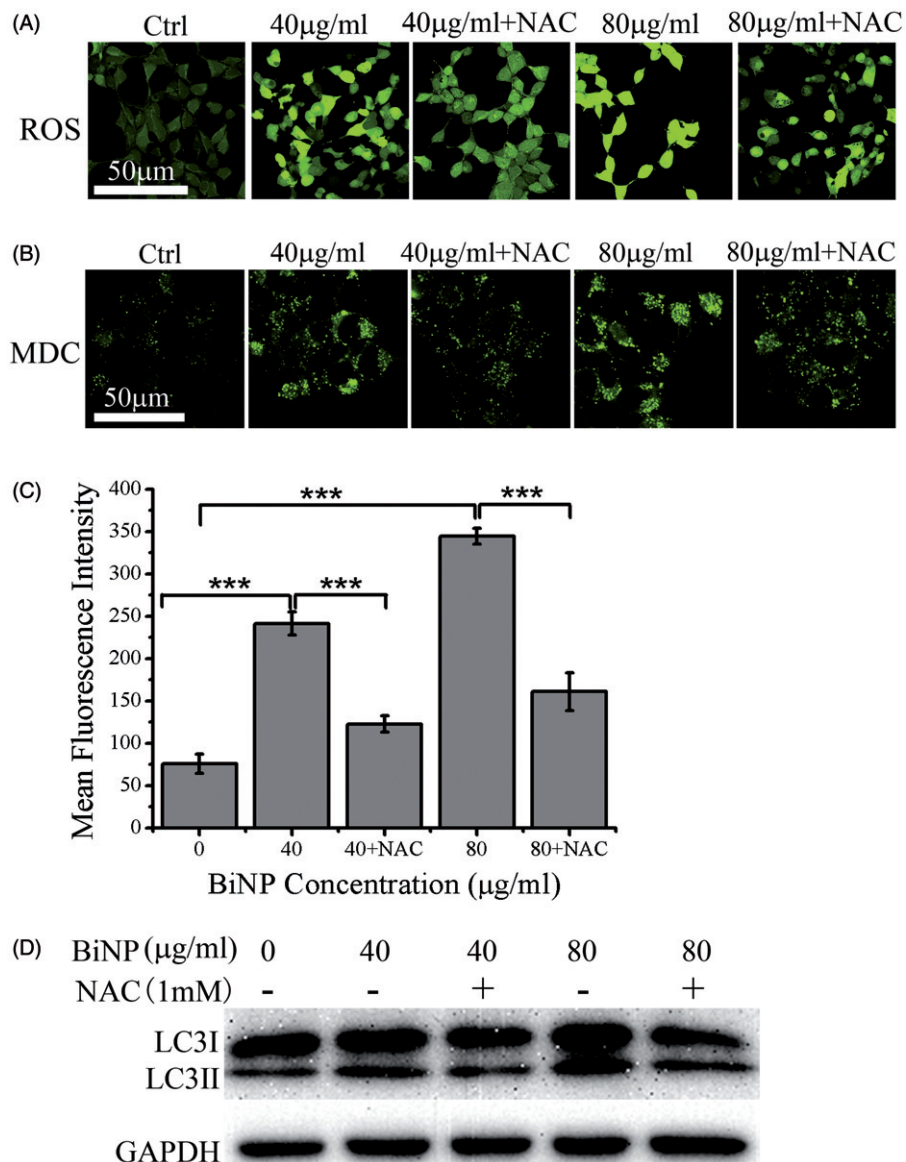


Figure 9. BiNP induced ROS contributes to autophagy in HEK293 cells. Cells were pretreated with or without ROS scavenger NAC for 1 h and co-treated with NAC and BiNP (40 and 80 µg/ml) for 24 h. (A) BiNP-induced generation of ROS was attenuated by NAC. Cells were treated with BiNP with/without NAC, stained with DCFH-DA and observed using CLSM. (B) ROS attenuation by NAC reduced BiNP induced autophagy. Cells were treated same as in (B), stained with monodansylcadaverine (MDC) and the fluorescence intensity observed in CLSM, analyzed and quantified by ImageJ, shown in (C), and LC3 expression was measured by western blotting analysis, which was presented in (D). All data for quantification represents means \pm SE from three independent experiments. *** p < 0.001.

To confirm whether BiNP can cause AKI, we measured blood biochemical parameters. BiNP significantly increased CREA, BUN and total protein level when mice were injected with BiNP, highly suggesting that BiNP caused AKI (Figure 2). In order to further confirm BiNP induced AKI, renal histopathological analysis was performed and demonstrated with apoptosis at low concentrations and necrocytosis/tubule cast at high concentrations (Figure 3). Some of the other metals also introduce moderate to severe kidney toxicity.

Silver possesses broad-spectrum antibacterial and minimal drug resistance properties; however, there have been reports that silver can induce kidney injury (Xu et al. 2012; Wen et al. 2017). In greater detail, silver nanoparticle (AgNP) was found to increase serum BUN level and histopathological observation showed silver-induced necrotic renal tubular epithelium with diffused hyaline degeneration. Silver can also induce injury in more organs, such as multifocal liver cell degeneration and necrosis (Wen et al. 2017). In our

current and previous studies, we realized that liver injury markers such as aspartate aminotransferase (AST) and alkaline phosphatase (ALP) and H&E staining had no change comparable to the control group (Wang et al. 2016). Therefore, we found that bismuth mainly induces kidney injury compared to other metal.

We demonstrated that BiNP induced autophagy *in vitro* and *in vivo*, with the evidence of the AV formation in TEM, LC3 punctate dots available in cytoplasm of LC3-overexpressing cells, and up-regulation of LC3II or other autophagic proteins initiated primarily through AMPK/mTOR pathway (Figures 4, 6, and 7). Interestingly, we found that BiNP was capable of causing autophagy at very low concentrations, suggesting the prompt adaption of kidney cells during slightly environmental changes (Figure S2). We also investigated the autophagic flux indicated by p62 protein profile and found that p62 protein had no change when the concentration of BiNP increased, indicating that BiNP only induced autophagy but had no influences on autophagic flux (Figure 6(C)).

A numerous of studies have found that metal compounds can induce ROS. Excessive ROS production leads to DNA damage, impairment of mitochondrial membrane potential and ER stress, all of which are the causes for autophagy that are Atg4 dependent (Park et al. 2012; Li et al. 2017). For example, silver NP can induce large amount of ROS production and the ratio of DNA fragmentation was also increased when the cells were treated with silver NP for 1 h. In addition, ROS was found to be associated with apoptosis induced by nanosilver and nanosilver-induced apoptosis was attenuated when ROS was inhibited (Hsin et al. 2008; Wang et al. 2017). There are evidence showed that ROS also participated in regulation of autophagy (Scherz-Shouval, Shvets, and Elazar 2007; Kaminsky and Zhivotovsky 2014). Therefore, here we further studied if BiNP can induce ROS in HEK293 cells, which could be responsible for autophagy initiation. We found that ROS was significantly increased when HEK293 cells were treated with BiNP (Figure 8). Autophagy caused by BiNP was attenuated when BiNP induced ROS was removed by NAC, a scavenger of ROS (Figures 6(C) and 9). We hypothesized that ROS induced autophagy and nephrotoxicity by BiNP may be associated each other.

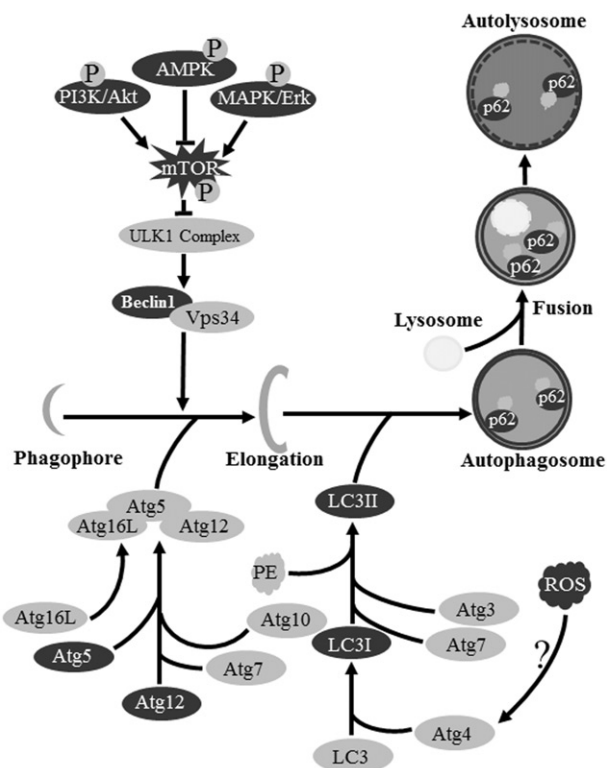


Figure 10. Overview of autophagy associated signal pathway and different autophagy stages induced by BiNP. In general, PI3K/Akt, MAPK/Erk, or AMPK all regulate autophagy process through mTOR. Here BiNP induced autophagy through AMPK phosphorylation and inhibits mTOR. The inhibition of the mTOR phosphorylation further introduced expression of Beclin1, likely due to the activation of ULK1 complex. The initiation of autophagy by Beclin1-Vps34 complex rearrange subcellular membranes to sequester a portion of cytoplasm and organelles into a structure called phagophore, which was facilitated by Atg12-Atg5 complex and other scaffold proteins. BiNP also introduced ROS, which helped with the formation of autophagic vacuoles likely through Atg4. Phagophore closure was formed by series of proteins including LC3, when LC3I was converted into LC3II by PE modification. Autophagosome further fused with lysosomes, forming autolysosomes which are responsible for the autophagic flux regulated by p62.

The upstream cell signal pathways to initiate autophagy usually involved with AMPK, PI3K/Akt, and MAPK/Erk, among which AMPK activation and inhibition of other two pathways can all lead to mTOR inhibition, resulting in autophagy initiation (Duan et al. 2014; Seo et al. 2016; He et al. 2017; Su et al. 2017). AMPK is an important kinase upstream of mTOR and negatively regulates mTOR activation. Cadmium is a toxic heavy metal and can cause autophagy via AMPK/mTOR signaling pathway (Son et al. 2011). In our study, we found that AMPK/mTOR signal pathway was also primarily responsible for induction of autophagy caused by BiNP.

With the increase in BiNP concentrations, p-AMPK level was significantly increased, and p-mTOR expression was decreased accordingly (Figure 7(A,E)). Other than AMPK, we detected a decrease in p-Akt by BiNP, while p-PI3K level remained unchanged, indicating the partial involvement of Akt in BiNP induced autophagy (Figure 7(B,C)). It should be noted that Atg5 expression level had no change when BiNP concentration increased (Figure 6(C)). During phagophore formation, Atg5 conjugates with Atg12 catalyzed by Atg7 and Atg10, two ligases to form Atg12-Atg5 conjugates, which further bind to Atg16L through interaction with Atg5, forming the Atg12-Atg5-Atg16L complex (Mizushima, Noda, and Ohsumi 1999; Kuma et al. 2002; Kim and Lee 2014). We hypothesize that Atg5 protein may be constitutively expressed as the adaptor protein to facilitate the formation of three protein-based complex, while Atg12 expression was more easily influenced by BiNP. Therefore, we suggested that autophagy induced by BiNP was mainly through AMPK/mTOR signaling pathway and partially regulated by Akt/mTOR, both of which facilitated the formation of Atg12-Atg5-Atg16L complex and PE modification of LC3II, resulting in phagophore closure and consequently, the autophagosome and autolysosome formation. The overall cell signaling pathways and stages for autophagy induction activated by BiNP were illustrated in Figure 10.

Conclusion

In summary, our study evidently demonstrated the toxicity of BiNP on kidney, resulting in increased CREA, BUN, and total protein. From the pathological point of view, apoptotic/necrotic PCT cells along with renal tubule casts were commonly observed. We also proved the occurrence of autophagy through AMPK/mTOR signaling pathway by BiNP, and ROS generated by BiNP was likely the initiator of autophagy. Other than mechanistic studies, we suggested that autophagy plays a protective role in BiNP induced AKI, which may help researchers better understand metal toxicity. Our study also provides fundamental theory and paved the way on the prevention of bismuth-induced nephrotoxicity during the clinical application of bismuth related compounds such as *Helicobacter pylori* eradication.

Disclosure statement

No potential conflict of interest was reported by the authors.

Funding

This work was supported by National Natural Science Foundation of China (#31771104, #81401511, #81373950, #51503139), Key Project of Natural Science Foundation of the Higher Education Institutions of Jiangsu Province (17KJA310003), Priority Academic Program Development of Jiangsu Higher Education Institutions (PAPD), and Jiangsu Provincial Key Laboratory of Radiation Medicine and Protection.

References

- İşlek, İ., S. Uysal, F. Gök, R. Dündaröz, and Ş. Küçük. 2001. "Reversible Nephrotoxicity after Overdose of Colloidal Bismuth Subcitrate." *Pediatric Nephrology* 16 (6): 510–514. doi:[10.1007/s004670100584](https://doi.org/10.1007/s004670100584).
- Andrews, P. C., G. B. Deacon, C. M. Forsyth, P. C. Junk, I. Kumar, and M. Maguire. 2006. "Towards a Structural Understanding of the Anti-Ulcer and Anti-Gastritis Drug Bismuth Subsaliicylate." *Angewandte Chemie International Edition* 45 (34): 5638–5642. doi:[10.1002/anie.200600469](https://doi.org/10.1002/anie.200600469).
- Azad, M. B., Y. Chen, and S. B. Gibson. 2009. "Regulation of Autophagy by Reactive Oxygen Species (ROS): Implications for Cancer Progression and Treatment." *Antioxidants and Redox Signaling* 11 (4): 777. doi:[10.1089/ars.2008.2270](https://doi.org/10.1089/ars.2008.2270).
- Caraciolo, G., F. Cardarelli, D. Pozzi, F. Salomone, G. Maccari, G. Bardi, A. L. Capriotti, C. Cavaliere, M. Papi, and A. Laganà. 2013. "Selective Targeting Capability Acquired with a Protein Corona Adsorbed on the Surface of 1,2-Dioleoyl-3-Trimethylammonium Propane/DNA Nanoparticles." *ACS Applied Materials and Interfaces* 5 (24): 13171–13179. doi:[10.1021/am404171h](https://doi.org/10.1021/am404171h).
- Chargui, A., S. Zekri, G. Jacquot, I. Rubera, M. Ilie, A. Belaid, C. Duranton, et al. 2011. "Cadmium-Induced Autophagy in Rat Kidney: An Early Biomarker of Subtoxic Exposure." *Toxicological Sciences* 121 (1): 31. doi:[10.1093/toxsci/kfr031](https://doi.org/10.1093/toxsci/kfr031).
- Chen, J., X. Q. Yang, M. Y. Qin, X. S. Zhang, Y. Xuan, and Y. D. Zhao. 2015. "Hybrid Nanoprobes of Bismuth Sulfide Nanoparticles and CdSe/ZnS Quantum Dots for Mouse Computed Tomography/Fluorescence Dual Mode Imaging." *Journal of Nanobiotechnology* 13 (1): 76. doi:[10.1186/s12951-015-0138-9](https://doi.org/10.1186/s12951-015-0138-9).
- Cheng, X., Y. Yong, Y. Dai, X. Song, G. Yang, Y. Pan, and C. Ge. 2017. "Enhanced Radiotherapy Using Bismuth Sulfide Nanoagents Combined with Photo-Thermal Treatment." *Theranostics* 7 (17): 4087–4098. doi:[10.7150/thno.20548](https://doi.org/10.7150/thno.20548).
- Cui, D., D. Sun, X. Wang, L. Yi, E. Kulikowicz, M. Reyes, J. Zhu, Z. J. Yang, W. Jiang, and R. C. Koehler. 2017. "Impaired Autophagosome Clearance Contributes to Neuronal Death in a Piglet Model of Neonatal Hypoxic-Ischemic Encephalopathy." *Cell Death and Disease* 8 (7): e2919. doi:[10.1038/cddis.2017.318](https://doi.org/10.1038/cddis.2017.318).

- Du, F., J. Lou, R. Jiang, Z. Fang, X. Zhao, Y. Niu, S. Zou, M. Zhang, A. Gong, and C. Wu. 2017. "Hyaluronic Acid-Functionalized Bismuth Oxide Nanoparticles for Computed Tomography Imaging-Guided Radiotherapy of Tumor." *International Journal of Nanomedicine* 12: 5973. doi:10.2147/IJNS130455.
- Duan, J., Y. Yu, Y. Yu, Y. Li, J. Wang, W. Geng, L. Jiang, Q. Li, X. Zhou, and Z. Sun. 2014. "Silica Nanoparticles Induce Autophagy and Endothelial Dysfunction via the PI3K/Akt/mTOR Signaling Pathway." *International Journal of Nanomedicine* 9 (1): 5131. doi:10.2147/IJN.S71074.
- Ferrari, M. 2005. "Cancer Nanotechnology: Opportunities and Challenges." *Nature Reviews Cancer* 5 (3): 161. doi:10.1038/nrc1566.
- Frake, R. A., T. Ricketts, F. M. Menzies, and D. C. Rubinsztein. 2015. "Autophagy and Neurodegeneration." *The Journal of Clinical Investigation* 125 (1): 65–74. doi:10.1172/JCI73944.
- Gao, X., Y. Wang, S. Peng, B. Yue, C. Fan, W. Chen, and X. Li. 2015. "Comparative Toxicities of Bismuth Oxybromide and Titanium Dioxide Exposure on Human Skin Keratinocyte Cells." *Chemosphere* 135: 83–93. doi:10.1016/j.chemosphere.2015.03.075.
- Guo, C., M. Yang, L. Jing, J. Wang, Y. Yu, Y. Li, J. Duan, X. Zhou, Y. Li, and Z. Sun. 2016. "Amorphous Silica Nanoparticles Trigger Vascular Endothelial Cell Injury through Apoptosis and Autophagy via Reactive Oxygen Species-Mediated MAPK/Bcl-2 and PI3K/Akt/mTOR Signaling." *International Journal of Nanomedicine* 11: 5257–5276. doi:10.2147/IJN.S112030.
- Gupta, A. K., and M. Gupta. 2005. "Synthesis and Surface Engineering of Iron Oxide Nanoparticles for Biomedical Applications." *Biomaterials* 26 (18): 3995–4014. doi:10.1016/j.biomaterials.2004.10.012.
- He, Y., H. She, T. Zhang, H. Xu, L. Cheng, M. Yepes, Y. Zhao, and Z. Mao. 2017. "p38 MAPK Inhibits Autophagy and Promotes Microglial Inflammatory Responses by Phosphorylating ULK1." *The Journal of Cell Biology* 217 (1): 315–328. doi:10.1083/jcb.201701049.
- Hsin, Y. H., C. F. Chen, S. Huang, T. S. Shih, P. S. Lai, and P. J. Chueh. 2008. "The Apoptotic Effect of Nanosilver is Mediated by a ROS- and JNK-Dependent Mechanism Involving the Mitochondrial Pathway in NIH3T3 Cells." *Toxicology Letters* 179 (3): 130–139. doi:10.1016/j.toxlet.2008.04.015.
- Jain, S., J. A. Coulter, A. R. Hounsell, K. T. Butterworth, S. J. McMahon, W. B. Hyland, M. F. Muir, et al. 2011. "Cell-Specific Radiosensitization by Gold Nanoparticles at Megavoltage Radiation Energies." *International Journal of Radiation Oncology Biology Physics* 79 (2): 531. doi:10.1016/j.ijrobp.2010.08.044.
- Joh, D. Y., L. Sun, M. Stangl, A. Al Zaki, S. Murty, P. P. Santoiemma, J. J. Davis, et al. 2013. "Selective Targeting of Brain Tumors with Gold Nanoparticle-Induced Radiosensitization." *PLoS One* 8 (4): e62425–e62520. doi:10.1371/journal.pone.0062425.
- Kaminskyy, V. O., and B. Zhivotovsky. 2014. "Free Radicals in Cross Talk between Autophagy and Apoptosis." *Antioxidants & Redox Signaling* 21 (1): 86–102. doi:10.1089/ars.2013.5746.
- Kang, C., L. Wei, B. Song, L. Chen, J. Liu, B. Deng, X. Pan, and L. Shao. 2017. "Involvement of Autophagy in Tantalum Nanoparticle-Induced Osteoblast Proliferation." *International Journal of Nanomedicine* 12: 4323–4333. doi:10.2147/IJN.S136281.
- Kawai, A., H. Uchiyama, S. Takano, N. Nakamura, and S. Ohkuma. 2007. "Autophagosome-Lysosome Fusion Depends on the pH in Acidic Compartments in CHO Cells." *Autophagy* 3 (2): 154–157. doi:10.4161/auto.3634.
- Kim, K. H., and M. S. Lee. 2014. "Autophagy-a Key Player in Cellular and Body Metabolism." *Nature Reviews Endocrinology* 10 (6): 322–337. doi:10.1038/nrendo.2014.35.
- Kinsella, J. M., R. E. Jimenez, P. P. Karmali, A. M. Rush, V. R. Kotamraju, N. C. Gianneschi, E. Ruoslahti, D. Stupack, and M. J. Sailor. 2011. "X-Ray Computed Tomography Imaging of Breast Cancer by Using Targeted Peptide-Labeled Bismuth Sulfide Nanoparticles." *Angewandte Chemie International Edition* 50 (51): 12308–12311. doi:10.1002/anie.201104507.
- Kuma, A., N. Mizushima, N. Ishihara, and Y. Ohsumi. 2002. "Formation of the Approximately 350-kDa Apg12-Apg5.Apg16 Multimeric Complex, Mediated by Apg16 Oligomerization, Is Essential for Autophagy in Yeast." *Journal of Biological Chemistry* 277 (21): 18619–18625. doi:10.1074/jbc.M111889200.
- Lavallard, V. J., A. J. Meijer, P. Codogno, and P. Gual. 2012. "Autophagy, Signaling and Obesity." *Pharmacological Research* 66 (6): 513. doi:10.1016/j.phrs.2012.09.003.
- Lavandero, S., R. Troncoso, B. A. Rothermel, W. Martinet, J. Sadoshima, and J. A. Hill. 2013. "Cardiovascular Autophagy: Concepts, Controversies, and Perspectives." *Autophagy* 9 (10): 1455–1466. doi:10.4161/auto.25969.
- Lee, J., S. Giordano, and J. Zhang. 2012. "Autophagy, Mitochondria and Oxidative Stress: Cross-Talk and Redox Signalling." *Biochemical Journal* 441 (2): 523–540. doi:10.1042/BJ20111451.
- Leussink, B. T., A. Slikkerveer, M. R. Engelbrecht, G. B. Van Der Voet, E. J. Nouwen, E. De Heer, M. E. De Broe, F. A. De Wolff, and J. A. Bruijn. 2001. "Bismuth Overdosing-Induced Reversible Nephropathy in Rats." *Archives of Toxicology* 74 (12): 745–754. doi:10.1007/s002040000190.
- Li, Z., Y. Hu, K. A. Howard, T. Jiang, X. Fan, Z. Miao, Y. Sun, F. Besenbacher, and M. Yu. 2016. "Multifunctional Bismuth Selenide Nanocomposites for Antitumor Thermo-Chemotherapy and Imaging." *ACS Nano* 10 (1): 984–997. doi:10.1021/acsnano.5b06259.
- Li, J., F. Jiang, B. Yang, X. R. Song, Y. Liu, H. H. Yang, D. R. Cao, W. R. Shi, and G. N. Chen. 2013. "Topological Insulator Bismuth Selenide as a Theranostic Platform for Simultaneous Cancer Imaging and Therapy." *Scientific Reports* 3 (1): 1998. doi:10.1038/srep01998.
- Li, B., M. Lu, X. X. Jiang, M. X. Pan, J. W. Mao, and M. Chen. 2017. "Inhibiting Reactive Oxygen Species-Dependent Autophagy Enhanced Baicalein-Induced Apoptosis in Oral

- Squamous Cell Carcinoma." *Journal of Natural Medicines* 71 (2): 433–441. doi:[10.1007/s11418-017-1076-7](https://doi.org/10.1007/s11418-017-1076-7).
- Liu, W., N. Dai, Y. Wang, C. Xu, H. Zhao, P. Xia, J. Gu, et al. 2016a. "Role of Autophagy in Cadmium-Induced Apoptosis of Primary Rat Osteoblasts." *Scientific Reports* 6 (1): 20404. doi:[10.1038/srep20404](https://doi.org/10.1038/srep20404).
- Liu, Y., Z. Jing, X. Zhang, L. Cong, Z. Ning, L. Yang, W. Yong, C. Tao, Y. Wang, and L. W. Zhang. 2017. "Autophagy Associated Cytotoxicity and Cellular Uptake Mechanisms of Bismuth Nanoparticles in Human Kidney Cells." *Toxicology Letters* 275: 39–48. doi:[10.1016/j.toxlet.2017.04.014](https://doi.org/10.1016/j.toxlet.2017.04.014).
- Liu, J., X. Zheng, L. Yan, L. Zhou, G. Tian, W. Yin, L. Wang, Y. Liu, Z. Hu, and Z. Gu. 2016b. "Bismuth Sulfide Nanorods as a Precision Nanomedicine for In Vivo Multimodal Imaging-Guided Photothermal Therapy of Tumor." *ACS Nano* 12 (2): 486–707. doi:[10.1016/j.nano.2015.12.116](https://doi.org/10.1016/j.nano.2015.12.116).
- Ma, X., R. J. Godar, H. Liu, and A. Diwan. 2012. "Enhancing Lysosome Biogenesis Attenuates BNIP3-Induced Cardiomyocyte Death." *Autophagy* 8 (3): 297–309. doi:[10.4161/auto.18658](https://doi.org/10.4161/auto.18658).
- Marcus, E. A., G. Sachs, and D. R. Scott. 2015. "Colloidal Bismuth Subcitrate Impedes Proton Entry into *Helicobacter pylori* and Increases the Efficacy of Growth-Dependent Antibiotics." *Alimentary Pharmacology and Therapeutics* 42 (7): 922–933. doi:[10.1111/apt.13346](https://doi.org/10.1111/apt.13346).
- Ma, X., Y. Wu, S. Jin, Y. Tian, X. Zhang, Y. Zhao, L. Yu, and X. J. Liang. 2011. "Gold Nanoparticles Induce Autophagosome Accumulation through Size-Dependent Nanoparticle Uptake and Lysosome Impairment." *ACS Nano* 5 (11): 8629–8639. doi:[10.1021/nn202155y](https://doi.org/10.1021/nn202155y).
- Mizushima, N., T. Noda, and Y. Ohsumi. 1999. "Apg16p Is Required for the Function of the Apg12p–Apg5p Conjugate in the Yeast Autophagy Pathway." *The Embo Journal* 18 (14): 3888–3896. doi:[10.1093/emboj/18.14.3888](https://doi.org/10.1093/emboj/18.14.3888).
- Munafó, D. B., and M. I. Colombo. 2001. "A Novel Assay to Study Autophagy: Regulation of Autophagosome Vacuole Size by Amino Acid Deprivation." *Journal of Cell Science* 114 (20): 3619–3629.
- Pankiv, S., T. H. Clausen, T. Lamark, A. Brech, J. A. Bruun, H. Outzen, A. Øvervatn, G. Bjørkøy, and T. Johansen. 2007. "p62/SQSTM1 Binds Directly to Atg8/LC3 to Facilitate Degradation of Ubiquitinated Protein Aggregates by Autophagy." *Journal of Biological Chemistry* 282 (33): 24131–24145. doi:[10.1074/jbc.M702824200](https://doi.org/10.1074/jbc.M702824200).
- Park, S., S. Kang, X. Chen, E. J. Kim, J. Kim, N. Kim, J. Kim, and M. M. Jin. 2013. "Tumor Suppression via Paclitaxel-Loaded Drug Carriers That Target Inflammation Marker Upregulated in Tumor Vasculature and Macrophages." *Biomaterials* 34 (2): 598–605. doi:[10.1016/j.biomaterials.2012.10.004](https://doi.org/10.1016/j.biomaterials.2012.10.004).
- Park, S. H., J. H. Kim, G. Y. Chi, G. Y. Kim, Y. C. Chang, S. K. Moon, S. W. Nam, W. J. Kim, Y. H. Yoo, and Y. H. Choi. 2012. "Induction of Apoptosis and Autophagy by Sodium Selenite in A549 Human Lung Carcinoma Cells through Generation of Reactive Oxygen Species." *Toxicology Letters* 212 (3): 252–261. doi:[10.1016/j.toxlet.2012.06.007](https://doi.org/10.1016/j.toxlet.2012.06.007).
- Pedro, B. S., F. Pietrocola, V. Sica, V. Izzo, A. Sauvat, O. Kepp, M. C. Maiuri, G. Kroemer, and L. Galluzzi. 2016. "High-Throughput Quantification of GFP-LC3 + Dots by Automated Fluorescence Microscopy." *Methods in Enzymology* 587: 71–86. doi:[10.1016/bs.mie.2016.10.022](https://doi.org/10.1016/bs.mie.2016.10.022).
- Scherz-Shouval, R., E. Shvets, and Z. Elazar. 2007. "Oxidation as a Post-Translational Modification That Regulates Autophagy." *Autophagy* 3 (4): 371–373. doi:[10.4161/auto.4214](https://doi.org/10.4161/auto.4214).
- Šebeková, K., M. Dušinská, K. Simon Klenovics, R. Kollárová, P. Boor, A. Kebis, M. Staruchová, et al. 2014. "Comprehensive Assessment of Nephrotoxicity of Intravenously Administered Sodium-Oleate-Coated Ultra-Small Superparamagnetic Iron Oxide (USPIO) and Titanium Dioxide (TiO₂) Nanoparticles in Rats." *Nanotoxicology* 8 (2): 142–157. doi:[10.3109/17435390.2012.763147](https://doi.org/10.3109/17435390.2012.763147).
- Seo, Y., Y. S. Cho, Y. D. Huh, and H. Park. 2016. "Copper Ion from Cu₂O Crystal Induces AMPK-Mediated Autophagy via Superoxide in Endothelial Cells." *Molecules and Cells* 39 (3): 195–203. doi:[10.14348/molcells.2016.2198](https://doi.org/10.14348/molcells.2016.2198).
- Son, Y. O., X. Wang, J. A. Hitron, Z. Zhang, S. Cheng, A. Budhraja, S. Ding, J. C. Lee, and X. Shi. 2011. "Cadmium Induces Autophagy through ROS-Dependent Activation of the LKB1-AMPK Signaling in Skin Epidermal Cells." *Toxicology & Applied Pharmacology* 255 (3): 287–296. doi:[10.1016/j.taap.2011.06.024](https://doi.org/10.1016/j.taap.2011.06.024).
- Song, G., Y. Chen, C. Liang, X. Yi, J. Liu, X. Sun, S. Shen, K. Yang, and Z. Liu. 2016. "Catalase-Loaded TaOx Nanoshells as Bio-Nanoreactors Combining High-Z Element and Enzyme Delivery for Enhancing Radiotherapy." *Advanced Materials* 28 (33): 7143–7148. doi:[10.1002/adma.201602111](https://doi.org/10.1002/adma.201602111).
- Su, R., X. Jin, W. Zhang, Z. Li, X. Liu, and J. Ren. 2017. "Particulate Matter Exposure Induces the Autophagy of Macrophages via Oxidative Stress-Mediated PI3K/AKT/mTOR Pathway." *Chemosphere* 167: 444–453. doi:[10.1016/j.chemosphere.2016.10.024](https://doi.org/10.1016/j.chemosphere.2016.10.024).
- Sutton, M. N., Yang, H. G. Y. Huang, C. Fu, M. Pontikos, Y. Wang, W. Mao, L. et al. 2018. "RAS-Related GTPases DIRAS1 and DIRAS2 Induce Autophagic Cancer Cell Death and are Required for Autophagy in Murine Ovarian Cancer Cells." *Autophagy* 21: 1–47. doi:[10.1080/15548627.2018.1427022](https://doi.org/10.1080/15548627.2018.1427022).
- Tanida, I. 2011. "Autophagy Basics." *Microbiology and Immunology* 55 (1): 1–11. doi:[10.1111/j.1348-0421.2010.00271.x](https://doi.org/10.1111/j.1348-0421.2010.00271.x).
- Taratula, O., A. Kuzmov, M. Shah, O. B. Garbuzenko, and T. Minko. 2013. "Nanostructured Lipid Carriers as Multifunctional Nanomedicine Platform for Pulmonary Co-Delivery of Anticancer Drugs and siRNA." *Journal of Controlled Release* 171 (3): 349–357. doi:[10.1016/j.conrel.2013.04.018](https://doi.org/10.1016/j.conrel.2013.04.018).
- Wang, E., Y. Huang, Q. Du, and Y. Sun. 2017. "Silver Nanoparticle Induced Toxicity to Human Sperm by Increasing ROS (Reactive Oxygen Species) Production and DNA Damage." *Environmental Toxicology and Pharmacology* 52: 193–199. doi:[10.1016/j.etap.2017.04.010](https://doi.org/10.1016/j.etap.2017.04.010).
- Wang, Q. W., Y. Wang, T. Wang, K. B. Zhang, Y. Yuan, J. C. Bian, X. Z. Liu, J. H. Gu, J. Q. Zhu, and Z. P. Liu. 2015. "Cadmium-Induced Autophagy Is Mediated by Oxidative Signaling in PC-12 Cells and Is Associated with

- Cytoprotection." *Molecular Medicine Reports* 12 (3): 4448–4454. doi:[10.3892/mmr.2015.3907](https://doi.org/10.3892/mmr.2015.3907).
- Wang, Y., Y. Wu, Y. Liu, J. Shen, L. Lv, L. Li, L. Yang, et al. 2016. "BSA-Mediated Synthesis of Bismuth Sulfide Nanotheranostic Agents for Tumor Multimodal Imaging and Thermoradiotherapy." *Advanced Functional Materials* 26 (29): 5335–5344. doi:[10.1002/adfm.201601341](https://doi.org/10.1002/adfm.201601341).
- Wen, H., M. Dan, Y. Yang, J. Lyu, A. Shao, X. Cheng, L. Chen, and L. Xu. 2017. "Acute Toxicity and Genotoxicity of Silver Nanoparticle in Rats." *PLoS One* 12 (9): e0185554. doi:[10.1371/journal.pone.0185554](https://doi.org/10.1371/journal.pone.0185554).
- White, E. 2015. "The Role for Autophagy in Cancer." *Journal of Clinical Investigation* 125 (1): 42–46. doi:[10.1172/JCI73941](https://doi.org/10.1172/JCI73941).
- Wu, Y. T., H. L. Tan, Q. Huang, C. N. Ong, and H. M. Shen. 2009. "Activation of the PI3K-Akt-mTOR Signaling Pathway Promotes Necrotic Cell Death via Suppression of Autophagy." *Autophagy* 5 (6): 824–834. doi:[10.4161/auto.9099](https://doi.org/10.4161/auto.9099).
- Xiao, Q., X. Zheng, W. Bu, W. Ge, S. Zhang, F. Chen, H. Xing, et al. 2013. "A Core/Satellite Multifunctional Nanotheranostic for In Vivo Imaging and Tumor Eradication by Radiation/Photothermal Synergistic Therapy." *Journal of the American Chemical Society* 135 (35): 13041–13048. doi:[10.1021/ja404985w](https://doi.org/10.1021/ja404985w).
- Xu, L., X. Li, T. Takemura, N. Hanagata, G. Wu, and L. Chou. 2012. "Genotoxicity and Molecular Response of Silver Nanoparticle (NP)-Based Hydrogel." *Journal of Nanobiotechnology* 10 (1): 16. doi:[10.1186/1477-3155-10-16](https://doi.org/10.1186/1477-3155-10-16).
- Zhang, X. D., J. Chen, Y. Min, G. B. Park, X. Shen, S. S. Song, Y. M. Sun, et al. 2014a. "Metabolizable Bi₂Se₃ Nanoplates: Biodistribution, Toxicity, and Uses for Cancer Radiation Therapy and Imaging." *Advanced Functional Materials* 24 (12): 1718–1729. doi:[10.1002/adfm.201302312](https://doi.org/10.1002/adfm.201302312).
- Zhang, X. D., Z. Luo, J. Chen, X. Shen, S. Song, Y. Sun, S. Fan, F. Fan, D. T. Leong, and J. Xie. 2014b. "Ultrasmall Au₁₀–12(SG)₁₀–12 Nanomolecules for High Tumor Specificity and Cancer Radiotherapy." *Advanced Materials* 26 (26): 4565–4568. doi:[10.1002/adma.201400866](https://doi.org/10.1002/adma.201400866).